

η - ^4He interaction from the $dd \rightarrow \eta^4\text{He}$ reaction near threshold

Ju-Jun Xie,^{1,*} Wei-Hong Liang,^{2,†} and Eulogio Oset^{3,‡}

¹*Institute of Modern Physics, Chinese Academy of Sciences, Lanzhou 730000, China*

²*Department of Physics, Guangxi Normal University, Guilin 541004, China*

³*Departamento de Física Teórica and IFIC, Centro Mixto Universidad de Valencia-CSIC
Institutos de Investigación de Paterna, Aptdo. 22085, 46071 Valencia, Spain*

(Dated: June 24, 2019)

We analyze the data on the total cross sections for the $dd \rightarrow \eta^4\text{He}$ reaction close to threshold and look for possible $\eta^4\text{He}$ bound states. We develop a framework in which the $\eta^4\text{He}$ optical potential is the key ingredient, rather than parameterizing the scattering matrix, as is usually done. The strength of this potential, together with some production parameters, are fitted to the available experimental data. The relationship of the scattering matrix to the optical potential is established using the Bethe-Salpeter equation and the $\eta^4\text{He}$ loop function incorporates the range of the interaction given by the experimental ^4He density. We find a bump structure in $|T|^2$ of the $\eta^4\text{He}$ amplitude T below threshold. However, when we look for poles of the scattering matrix, with the fits of high precision, we get poles in the bound region, poles in the positive energy region or no poles at all. We can quantize the probability to find poles in the bound region in 62%.

PACS numbers: 21.85.+d, 14.40.Aq, 13.75.-n

I. INTRODUCTION

The search for η bound states in nuclei has been a constant thought for several years [1–6], starting from the early works of Refs. [7–9]. Follow up evaluations of the η -nucleus optical potential, with special attention to two-nucleon η absorption, showed that, and while indeed the ηN interaction was strong enough to bind η states, the widths were always bigger than the binding [10].

The η -nucleus interaction within the chiral unitary approach was studied in Ref. [11], where enough attraction was found to form bound η -nucleus states. Detailed studies of the η energies for different nuclei were made in Ref. [12] where, for medium and light nuclei, bound states were found (see also Ref. [13], where qualitatively similar conclusions were drawn), though with larger widths than binding energies. For instance, some theoretical calculations for light systems predicted binding energy B_E of around 1 MeV or less and width $\Gamma = 15$ MeV for $\eta^3\text{He}$ [14]. In the recent work [15] the results of Ref. [14] have been updated, in particular the width results much smaller. In Ref. [16], the data on cross sections and asymmetries for the $pd \rightarrow \eta^3\text{He}$ reaction close to threshold were studied with the aim looking for bound states of the $\eta^3\text{He}$ system. The resulting $\eta^3\text{He}$ scattering matrix had a local Breit-Wigner form in a narrow range of energies which corresponded to a binding of about 0.3 MeV and a width of about 3 MeV. However, the pole appeared in the continuum, not in the bound region.

The fact that the widths are expected to be much larger than the binding might be the reason why so far, we have no con-

clusive evidence for any of these bound states [17–37].

The first measurements of the $dd \rightarrow \eta^4\text{He}$ total cross sections were carried out using the SPES4 [21] and the SPES3 [22] spectrometers at SATURNE. Later on, the $dd \rightarrow \eta^4\text{He}$ reaction has been investigated near threshold using the ANKE facility [23]. The total cross sections have been measured at two excess energies, $Q = 2.6$ and 7.7 MeV. The data on the $dd \rightarrow \eta^4\text{He}$ total cross section show a clear enhancement from threshold before becoming stable at an excess energy of about $Q = 3$ MeV, keeping this constant value up to about 10 MeV [22]. Recently, the search for $\eta^4\text{He}$ bound state of the $dd \rightarrow (\eta + ^4\text{He})_{\text{bound}} \rightarrow X$ reaction has been proposed and performed at the WASA-at-COSY facility [24–29]. These measurements have been analyzed in Ref. [38] within a theoretical model. The authors of Ref. [38] used a phenomenological method with an optical potential for the η - ^4He interaction. The available data on the $dd \rightarrow \eta^4\text{He}$ reaction is reproduced quite well for a broad range of optical potential parameters for some of which the authors predicted the η - ^4He bound state formation in the subthreshold region. Furthermore, the theoretical calculations of Ref. [38] were compared with the experimental data below the η production threshold, with the WASA-at-COSY excitation functions for the $dd \rightarrow ^3\text{He}N\pi$ reactions in Ref. [39], where no clear signal of the $\eta^4\text{He}$ bound state was found. As a consequence, the analysis in Ref. [39] made further strong constraints on the η - ^4He optical potential. With the results obtained in Ref. [39], most predictions of an $\eta^4\text{He}$ bound state seem to be excluded.

In the present work, we use an alternative method of analysis, following the algorithms used in the chiral unitary approach. This allows one to produce an $\eta^4\text{He}$ amplitude that is fully unitary and with proper analytical properties, making only basic assumptions. Our approach does not assume any particular form of the amplitude, instead it is generated from an $\eta^4\text{He}$ potential which is fitted to the data. The T -matrix then arises from the solution of the Lippmann-Schwinger

*Electronic address: xiejujun@impcas.ac.cn

†Electronic address: liangwh@gxnu.edu.cn

‡Electronic address: oset@ific.uv.es

equation, although we use the Bethe-Salpeter equation (BSE) for convenience, which allows us to keep relativistic terms.

We relate the parameters of the potential to the ηN scattering length $a_{\eta N}$ and this provides a valuable constraint. As we shall see later, the output of our calculations leads to an $\eta^4\text{He}$ optical potential from which we deduce a value of $a_{\eta N}$ that is basically consistent with experimental information. With this optical potential we solve the BSE for the $\eta^4\text{He}$ system and find an amplitude that has a broad peak with its maximum below threshold and close to it. However, when looking for poles of the amplitude, they either do not show up or appear in the bound or unbound region for the range of allowed parameters of the fitted potential.

Steps in a similar direction to ours were taken in Ref. [38], where the available data on the $dd \rightarrow \eta^4\text{He}$ reaction were studied in terms of optical potentials. The results obtained here are similar to those obtained in that work.

II. FORMALISM

In this section, we consider the $dd \rightarrow \eta^4\text{He}$ reaction and explain our theoretical approach developed in the present work. In Fig. 1 we depict diagrammatically the $dd \rightarrow \eta^4\text{He}$ process.

A. The $\eta^4\text{He}$ interaction

The $\eta^4\text{He} \rightarrow \eta^4\text{He}$ scattering amplitude is given by the diagrams shown in Fig. 2, and formally by the BSE

$$T = V + VGT, \quad (1)$$

where G is the loop function of intermediate states, and V is the $\eta^4\text{He}$ optical potential, which contains an imaginary part to account for the inelastic channels $\eta^4\text{He} \rightarrow X$ with X being mostly $\pi^3\text{He}N$. It also includes the $^3\text{He}N^*(1535)$ intermediate state arising mainly from the η meson absorption, $\eta N \rightarrow N^*(1535)$ [29].

The low density theorem in many-body theory tells us that at low densities the optical potential is given by,

$$V(\vec{r}) = 4t_{\eta N}\tilde{\rho}(\vec{r}), \quad (2)$$

where $t_{\eta N}$ is the forward ηN amplitude and $\tilde{\rho}(\vec{r})$ is the ^4He density normalized to unity. Eq. (2) is relatively accurate in many body physics, but here we do not use it. We only take from it the density dependence which provides a realistic range of the η -nucleus interaction, since the η can interact with all the nucleons in the nucleus distributed according to $\rho(\vec{r})$.

In momentum space the potential is given by

$$\begin{aligned} V(\vec{p}_\eta, \vec{p}'_\eta) &= 4t_{\eta N} \int d^3\vec{r} \tilde{\rho}(\vec{r}) e^{i(\vec{p}_\eta - \vec{p}'_\eta) \cdot \vec{r}} \\ &= 4t_{\eta N} F(\vec{p}_\eta - \vec{p}'_\eta), \end{aligned} \quad (3)$$

where $F(\vec{q})$ is the ^4He form factor,

$$F(\vec{q}) = \int d^3\vec{r} \tilde{\rho}(\vec{r}) e^{i\vec{q} \cdot \vec{r}}, \quad (4)$$

and $F(\vec{0}) = 1$. A good approximation to this form factor at small momentum transfers is given by a Gaussian,

$$F(\vec{q}) = e^{-\beta^2|\vec{q}|^2}, \quad (5)$$

where $\beta^2 = \langle r^2 \rangle / 6$. This mean-square radius corresponds to the distribution of the centers of the nucleons and, after correcting for the nucleon size, it leads to an experimental value of $\beta^2 = 12.1 \text{ GeV}^{-2}$ which was obtained with $\langle r^2 \rangle_{^4\text{He}}^{1/2} = 1.68 \text{ fm}$ as in Ref. [40].

Because of this form factor, the optical potential in Eq. (3) contains all partial waves. After integrating over the angle between \vec{p}'_η and \vec{p}_η , the s -wave projection of the optical potential becomes

$$\begin{aligned} V(\vec{p}_\eta, \vec{p}'_\eta) &= 4t_{\eta N} \frac{1}{2} \int_{-1}^1 d\cos\theta e^{-\beta^2(|\vec{p}_\eta|^2 + |\vec{p}'_\eta|^2 - 2|\vec{p}_\eta||\vec{p}'_\eta|\cos\theta)} \\ &= 4t_{\eta N} e^{-\beta^2|\vec{p}_\eta|^2} e^{-\beta^2|\vec{p}'_\eta|^2} \left[1 + \frac{1}{6}(2\beta^2|\vec{p}_\eta||\vec{p}'_\eta|)^2 + \dots \right]. \end{aligned} \quad (6)$$

One can easily see that the terms $(2\beta^2|\vec{p}_\eta||\vec{p}'_\eta|)^2/6 + \dots$ are negligible in the region where $e^{-\beta^2|\vec{p}_\eta|^2} e^{-\beta^2|\vec{p}'_\eta|^2}$ is sizeable and this leads to a potential that is separable in the variables \vec{p}_η and \vec{p}'_η , which makes the solution of Eq. (1) trivial. Keeping the relativistic factors of the BSE, we can write [41]:

$$\begin{aligned} T(\vec{p}_\eta, \vec{p}'_\eta) &= \tilde{V} e^{-\beta^2|\vec{p}_\eta|^2} e^{-\beta^2|\vec{p}'_\eta|^2} + \\ &\int \frac{d^3\vec{q}}{(2\pi)^3} \frac{M_{^4\text{He}}}{2\omega_\eta(\vec{q})E_{^4\text{He}}(\vec{q})} \frac{\tilde{V} e^{-\beta^2|\vec{p}_\eta|^2} e^{-\beta^2|\vec{q}|^2}}{\sqrt{s} - \omega_\eta(\vec{q}) - E_{^4\text{He}}(\vec{q}) + i\epsilon} T(\vec{q}, \vec{p}'_\eta), \end{aligned} \quad (7)$$

with \sqrt{s} being the invariant mass of the $\eta^4\text{He}$ system, $\omega_\eta(\vec{q}) = \sqrt{m_\eta^2 + |\vec{q}|^2}$, and $E_{^4\text{He}}(\vec{q}) = \sqrt{M_{^4\text{He}}^2 + |\vec{q}|^2}$. Note that we have here taken \tilde{V} instead of $4t_{\eta N}$ for more generality.

The T matrix can be factorized in the same way as V , and we have [16]

$$T(\vec{p}_\eta, \vec{p}'_\eta) = t e^{-\beta^2|\vec{p}_\eta|^2} e^{-\beta^2|\vec{p}'_\eta|^2}. \quad (8)$$

The BSE becomes then algebraic

$$t = \tilde{V} + \tilde{V}Gt, \quad (9)$$

with loop function

$$\begin{aligned} G(\sqrt{s}) &= \frac{M_{^4\text{He}}}{16\pi^3} \times \\ &\int \frac{d^3\vec{q}}{\omega_\eta(\vec{q})E_{^4\text{He}}(\vec{q})} \frac{e^{-2\beta^2|\vec{q}|^2}}{\sqrt{s} - \omega_\eta(\vec{q}) - E_{^4\text{He}}(\vec{q}) + i\epsilon}. \end{aligned} \quad (10)$$

In Fig. 3, we show the real and imaginary parts of the loop function G as a function of the excess energy Q ($Q = \sqrt{s} - m_\eta - M_{^4\text{He}}$) with $M_{^4\text{He}} = 3728.4 \text{ MeV}$ and $m_\eta = 547.862 \text{ MeV}$. We can see a strong cusp of the real part at the $\eta^4\text{He}$ threshold and the imaginary part starting from this threshold.

In the normalization that we are using, the η -nucleon and $\eta^4\text{He}$ scattering lengths are related to the t -matrices by

$$a_{\eta N} = \frac{1}{4\pi} \frac{m_N}{\sqrt{s_{\eta N}}} t_{\eta N} \Big|_{\sqrt{s_{\eta N}} = m_N + m_\eta} \quad (11)$$

$$a_{\eta^4\text{He}} = \frac{1}{4\pi} \frac{M_{^4\text{He}}}{\sqrt{s}} T \Big|_{\sqrt{s} = M_{^4\text{He}} + m_\eta}. \quad (12)$$

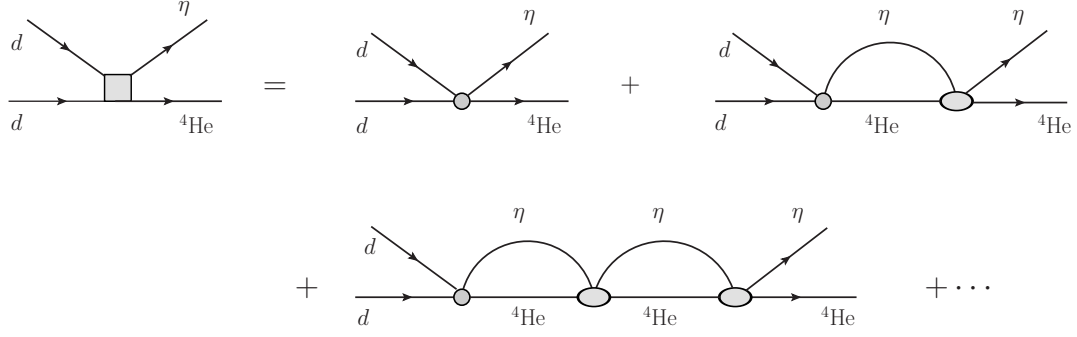


FIG. 1: The process $dd \rightarrow \eta^4\text{He}$ considering explicitly the $\eta^4\text{He}$ re-scattering. The square box in the first diagram indicates the full transition amplitude, while the circle in the second diagram stands for the bare transition amplitude prior to the $\eta^4\text{He}$ final state interaction. It contains all diagrams that do not have $\eta^4\text{He}$ as intermediate state. The oval stands for the $\eta^4\text{He}$ optical potential.

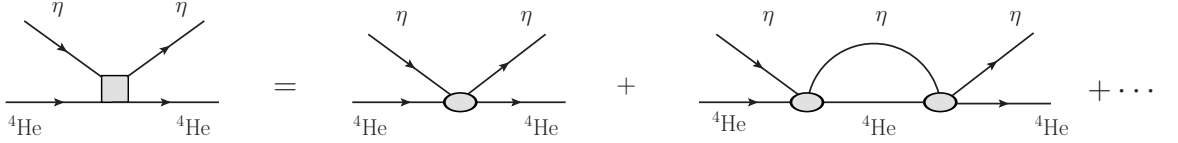


FIG. 2: Diagrammatic representation of the $\eta^4\text{He} \rightarrow \eta^4\text{He}$ scattering matrix.

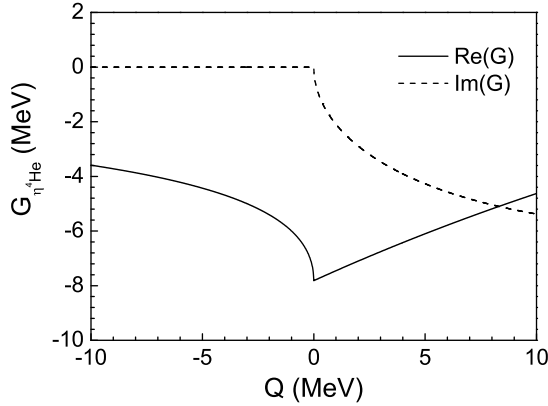


FIG. 3: Real (solid line) and imaginary (dashed line) parts of the G of Eq. (10) as functions of the excess energy Q .

The strategy that we adopt is to fit \tilde{V} to the $dd \rightarrow \eta^4\text{He}$ data and then see how different \tilde{V} is from $4t_{\eta N}$ by evaluating

$$a'_{\eta N} = \frac{1}{4\pi} \frac{m_N}{\sqrt{s_{\eta N}}} \frac{\tilde{V}}{4} \bigg|_{\sqrt{s_{\eta N}}=m_N+m_\eta} \quad (13)$$

and comparing it to the theoretical value of $a_{\eta N}$.

After obtaining the *best* value for \tilde{V} , we then plot

$$T = te^{-2\beta^2|\vec{p}_\eta|^2} \quad (14)$$

and investigate $|T|^2$ below threshold to identify a bump and its width. From this we can determine roughly the position and width of the bound state. A more precise determination is

done by plotting $\text{Re}(t)$ and $\text{Im}(t)$, and we see that in a narrow range of Q they are consistent with a Breit-Wigner form

$$t = \frac{g^2}{\sqrt{s} - M_R + i\Gamma/2} = \frac{g^2(\sqrt{s} - M_R)}{(\sqrt{s} - M_R)^2 + \Gamma^2/4} - i \frac{g^2\Gamma/2}{(\sqrt{s} - M_R)^2 + \Gamma^2/4}, \quad (15)$$

where g is constant and M_R and Γ are the mass and width of the $\eta^4\text{He}$ bound state.

B. Production amplitude

Following the formalism of Refs. [23, 38], we write for the $dd \rightarrow \eta^4\text{He}$ transition depicted as a circle in Fig. 1

$$V_P = A(\vec{\epsilon}_1 \times \vec{\epsilon}_2) \cdot \vec{p}_d, \quad (16)$$

where $\vec{\epsilon}_1$ and $\vec{\epsilon}_2$ are the polarizations of the initial two deuterons, and \vec{p}_d is the momentum in the initial state. This amplitude has the initial-state p -wave needed to match the $\eta(0^-)^4\text{He}(0^+)$ with the $d(1^+)d(1^+)$ system.

With similar arguments to those used to derive Eq. (3), we can justify that V_P in Eq. (16) must be accompanied by the factor $e^{-\beta^2|\vec{p}_\eta|^2}$, which, if the η is in the loop, will become $e^{-\beta^2|\vec{q}|^2}$. In view of this we can write analytically the equation for the diagrams of Fig. 1 as,

$$\begin{aligned} t_{dd \rightarrow \eta^4\text{He}} &= V_P e^{-\beta^2|\vec{p}_\eta|^2} + V_P G t e^{-\beta^2|\vec{p}_\eta|^2} \\ &= V_P e^{-\beta^2|\vec{p}_\eta|^2} (1 + Gt) = \frac{V_P e^{-\beta^2|\vec{p}_\eta|^2}}{1 - \tilde{V}G}, \end{aligned} \quad (17)$$

where in the last step we have used Eq. (1). The cross section then becomes

$$\sigma = \frac{M_d^2 M_{\eta^4\text{He}}}{9\pi s} \frac{|A|^2}{|1 - \tilde{V}G|^2} |\vec{p}_\eta||\vec{p}_d| e^{-2\beta^2|\vec{p}_\eta|^2}, \quad (18)$$

where we have used

$$\sum \sum |V_P|^2 = \frac{2}{9} |A|^2 |\vec{p}_d|^2. \quad (19)$$

This allows us to perform a fit to the data up to an excess energy $Q = 10$ MeV, and thus determine \tilde{V} . From this we shall determine T by means of Eqs. (8) and (9), and investigate its structure below threshold.

III. RESULTS

We perform a three-parameter $[|A| = r_A \text{ and } \tilde{V} = \text{Re}(V) + i\text{Im}(V)] \chi^2$ fit to the experimental data on the total cross sections of the $dd \rightarrow \eta^4\text{He}$ reaction below $Q = 10$ MeV. There are 12 experimental data points in total. The values of the resulting parameters are collected in Table I. One can see that the fitted parameters have large uncertainties, especially for the real part of \tilde{V} .

TABLE I: Values of parameters determined in this work.

Parameter	Fitted value
$r_A [\text{MeV}^{-5/2}]$	$(7.6 \pm 2.3) \times 10^{-9}$
$\text{Re}(V) [\text{MeV}^{-1}]$	$(-12.3 \pm 18.4) \times 10^{-2}$
$\text{Im}(V) [\text{MeV}^{-1}]$	$(-13.7 \pm 5.4) \times 10^{-2}$

To get more precise information from the experimental measurements, we generate random sets of the experimental data within the range of error of each datum. For each set of data, we perform a χ^2 fit, and the corresponding fitted parameters are determined by the best fit. In this way, we get sets of the fitted parameters (r_A , $\text{Re}(V)$, $\text{Im}(V)$) with different best χ^2_{best} . The minimum χ^2 that we get from the best fits is 0.12. Then we choose these sets of the fitted parameters, such that the corresponding χ^2_{best} is only increased below $\chi^2_{\text{min}} + 0.35$ ¹. With these best fits we get the shaded region² shown in Fig. 4, from where one can see that the experimental data can be well reproduced. Besides, in Fig. 4 we also show the fitted total cross sections with the centroid values of the fitted parameters listed in Table I by the red-solid curve.

On the other hand, as is general in particle physics, and in particular in the case of the $\eta^4\text{He}$ scattering matrix, the position of the poles of T does not coincide with that of the mass and width of a possible Breit-Wigner parametrization. We investigate the position of the poles here. In table II we show

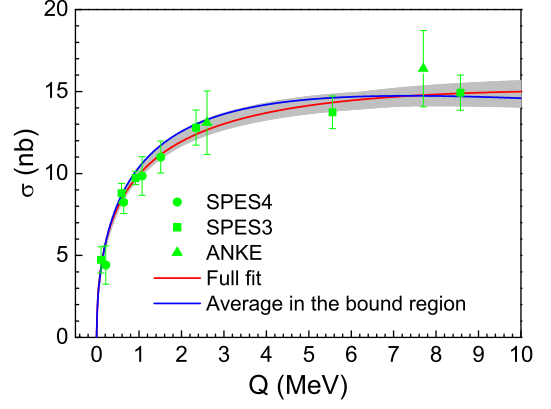


FIG. 4: The fitted $dd \rightarrow \eta^4\text{He}$ total cross sections compared with experimental data. The circles are taken from Ref. [21]; squares are from Ref. [22]; and triangles are from Ref. [23]. The band is obtained by removing 16% of the upper lines and 16% of the lower lines [42].

the position of the poles ($z_R = E - i\Gamma/2$) with the energy E measured from the $\eta^4\text{He}$ threshold.

We can see that for the centroid values of \tilde{V} in table I we get a pole in the unbound region around 10.6 MeV and with Γ around 11.4 MeV. Stretching the errors in $\text{Re}(V)$ in table I, if we take $\text{Re}(V) = -0.2 \text{ MeV}^{-1}$ and $\text{Im}(V) = -0.1 \text{ MeV}^{-1}$ we find now a pole with E around -0.4 MeV and width Γ of about 16.2 MeV. To complete the table we show what happens if we increase $\text{Re}(V)$ in size in the range of table I. For $\text{Re}(V) = -0.24 \text{ MeV}^{-1}$ and $\text{Im}(V) = -0.1 \text{ MeV}^{-1}$ we find already a bound state around $E = -4.5 \text{ MeV}$ and with a width Γ of about 19.2 MeV. In conclusion, because of the limited experimental data, we cannot always find a bound state with the fitted potential, which coincides with the conclusion of Ref. [16] for $\eta^3\text{He}$ and the conclusions of Refs. [38, 39].

We also observe the general trend that the widths are bigger than the binding.

TABLE II: Pole position of the T matrix for the $\eta^4\text{He} \rightarrow \eta^4\text{He}$ scattering.

$\text{Re}(V) [\text{MeV}^{-1}]$	$\text{Im}(V) [\text{MeV}^{-1}]$	$E [\text{MeV}]$	$\Gamma [\text{MeV}]$
-0.123	-0.137	10.0	13.3
-0.2	-0.15	2.0	26.9
-0.2	-0.1	-0.4	16.2
-0.22	-0.1	-2.4	17.8
-0.24	-0.1	-4.5	19.2
-0.26	-0.1	-6.6	20.4
-0.26	-0.08	-7.2	16.1
-0.26	-0.06	-7.6	11.9
-0.26	-0.04	-7.9	7.9
-0.28	-0.1	-8.9	21.4

In order to understand the results of our analysis more clearly, we plot three areas inside the $\text{Re}(V)$ - $\text{Im}(V)$ plane as

¹ The value of 0.35 is obtained for the region of 95% confidence level (see more details in Ref. [42]).

² The band does not change much when we take the region of the confidence level larger than 80% choosing all best fits with $\chi^2 < \chi^2_{\text{min}} + 1$.

shown in Fig. 5, where the acceptable region of $\text{Re}(V)$ and $\text{Im}(V)$ values can be easily understood for having an $\eta^4\text{He}$ bound state. The poles in areas I and II are in the unbound and bound regions, respectively, while there is no pole in area III.

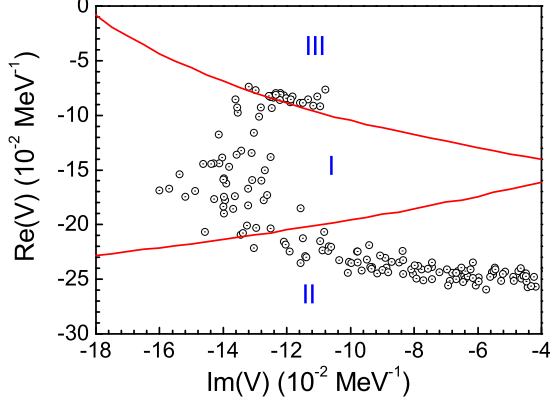


FIG. 5: Poles area in the $\text{Re}(V)$ - $\text{Im}(V)$ plane, where the circles are the best fitted pairs of $[\text{Re}(V), \text{Im}(V)]$.

In Fig. 5, we show also the fitted results of the pairs of $\text{Re}(V)$ and $\text{Im}(V)$, which correspond to those best fits as discussed above. For these $[\text{Re}(V), \text{Im}(V)]$ sets in area II, we get 118 pairs compared with the total 190 pairs shown in Fig. 5, which indicates that 62% of the best fits are in the bound region. To understand more clearly the best fits that lie in the bound region, we get the average value of $\bar{V} = \text{Re}(V) + i\text{Im}(V) = (-24.1 - i6.6) \times 10^{-2} \text{ MeV}^{-1}$, which is obtained from these $(\text{Re}(V), \text{Im}(V))$ pairs in area II, and the corresponding \bar{r}_A is $6.9 \times 10^{-9} \text{ MeV}^{-5/2}$. We show the total cross sections obtained with the above values in Fig. 4 by the blue-solid curve. We see that it can also describe the experimental data quite well. Furthermore, with the value of \bar{V} , we get a bound $\eta^4\text{He}$ state with $B_E = 5.5 \text{ MeV}$ and $\Gamma = 12.3 \text{ MeV}$.

On the other hand, with the potentials \tilde{V} obtained from the best fits as shown in Fig. 5, we have evaluated the scattering length $a'_{\eta N}$ of Eq. (13):

$$a'_{\eta N} = [-(0.5 \pm 0.1) - i(0.2 \pm 0.1)] \text{ fm}, \quad (20)$$

which is comparable with the value obtained in Ref. [16] within errors. The errors quoted here are statistical and they are determined as the standard deviation.

Similarly, by means of Eq. (12), we calculate the $\eta^4\text{He}$ scattering length to be

$$a_{\eta^4\text{He}} = [(2.6 \pm 0.8) - i(1.1 \pm 0.4)] \text{ fm}. \quad (21)$$

The value of $a_{\eta^4\text{He}}$ obtained here is different from the results obtained in Refs. [22, 23, 38], while the absolute value of $a_{\eta^4\text{He}}$ is compatible with the results of these works.

Note that the strategy of fitting an optical potential to the data instead of the usual t -matrix parametrization used in pre-

vious works, allows us to determine the sign of the real part of the scattering lengths.

The fit done here produces an attractive potential, which is consistent with all theoretical derivations of $t_{\eta N}$, together with the $t_{\eta N}\tilde{\rho}(\vec{r})$ assumption for the optical potential.

We next turn our attention to the $\eta^4\text{He} \rightarrow \eta^4\text{He}$ scattering amplitude. We first show the numerical results for the $|T|^2$ with two models: Model I takes the potentials with which we obtained the band for the $dd \rightarrow \eta^4\text{He}$ total cross sections as shown in Fig. 4; Model II takes the potentials in the bound region of Model I. In Figs. 6 and 7, we depict $|T|^2$ obtained with Models I and II, respectively. We see a clear bump structure below the $\eta^4\text{He}$ threshold, which is tied to the fast increase of the $dd \rightarrow \eta^4\text{He}$ cross sections close to the reaction threshold.

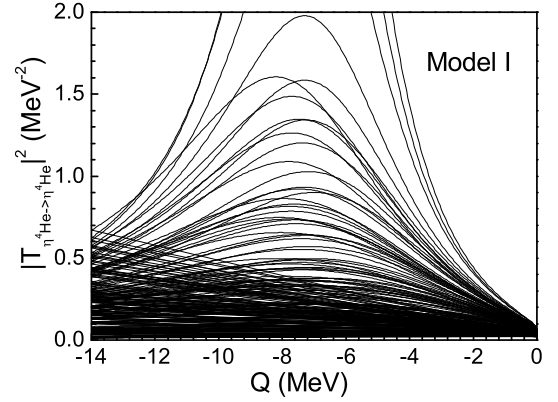


FIG. 6: Square of the absolute value of the $\eta^4\text{He} \rightarrow \eta^4\text{He}$ scattering amplitude. Results are obtained with Model I.

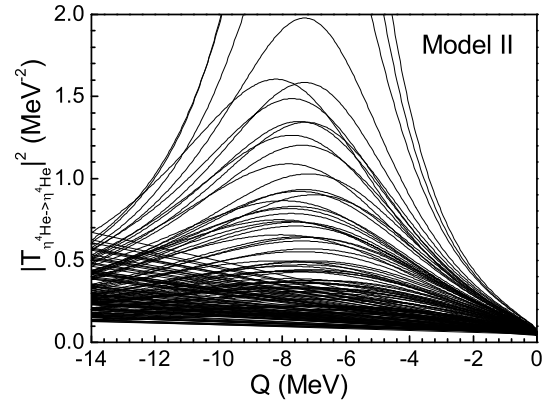


FIG. 7: As in Fig. 6 but for the results obtained with Model II.

In order to make more quantitative statements, we plot in Figs. 8 and 9 the real and imaginary parts of T obtained with Models I and II, respectively. We see that around $Q = -7 \text{ MeV}$, $\text{Re}(T)$ goes from negative to positive passing through zero, $\text{Im}(T)$ is negative, and $-\text{Im}(T)$ has a peak. This indi-

cates that around $Q = -7$ MeV the $\eta^4\text{He} \rightarrow \eta^4\text{He}$ scattering amplitude has the simple Breit-Wigner form with mass M_R corresponding to a binding energy about 7 MeV.

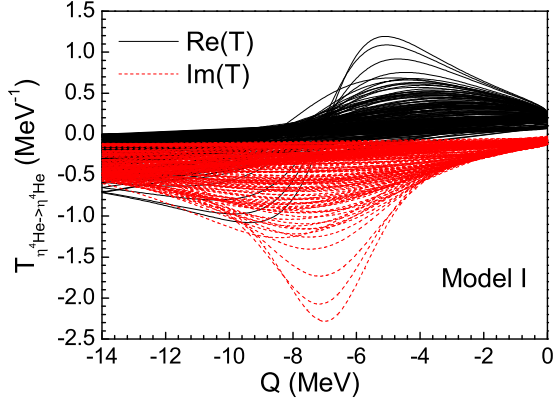


FIG. 8: (color online) Real and imaginary parts of the $\eta^4\text{He} \rightarrow \eta^4\text{He}$ amplitude T as a function of the excess energy Q . Results are obtained with Model I.

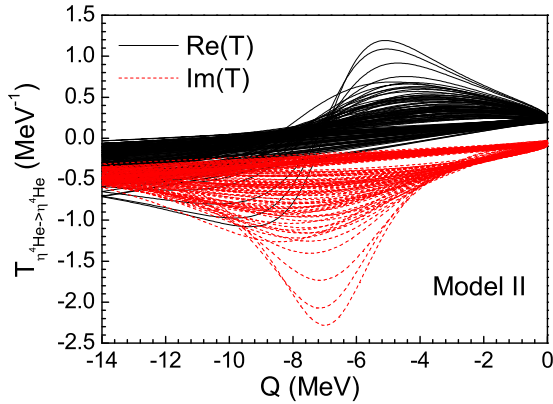


FIG. 9: As in Fig. 8 but for the results obtained with Model II.

Independent of the possible parametrization of the amplitude as a local Breit-Wigner in a narrow region of energies, the results of Figs. 8 and 9 indicate that there is a structure of the amplitude below threshold and close to it. Comparison of this structure with the one found for $|T|^2$ of $\eta^3\text{He} \rightarrow \eta^3\text{He}$ scattering in Ref. [16] indicates that it peaks at lower energies than in Ref. [16] and is also broader. This is reflected in the $dd \rightarrow \eta^4\text{He}$ cross section just above threshold, which is not as steep as in the $pd \rightarrow \eta^3\text{He}$ reaction. Just from this experimental fact one could clearly guess, as it finally comes out, that the structure of $|T|^2$ for $\eta^4\text{He} \rightarrow \eta^4\text{He}$ below threshold would peak at lower energies than for $\eta^3\text{He}$ or would be wider. The results obtained tell us that both things happen.

One should also note that in Ref. [16] one not only fitted the $pd \rightarrow \eta^3\text{He}$ total cross sections but also the asymmetry parameter in terms of the η momentum. Also the quality of

the data of $pd \rightarrow \eta^3\text{He}$ reaction is much better than for the present reaction. As a consequence, we could determine the parameters in the case of the $\eta^3\text{He}$ interaction with more precision than in the present case.

IV. SUMMARY AND CONCLUSIONS

We have performed an analysis of the total cross sections data on the $dd \rightarrow \eta^4\text{He}$ reaction close to threshold. Unlike former approaches that make a parametrization of the amplitude, we express the total cross sections in terms of an optical potential from which the $\eta^4\text{He}$ scattering amplitude is evaluated. The T matrix is evaluated from the potential using the Bethe-Salpeter equation and the loop function G of the intermediate $\eta^4\text{He}$ state. This reflects the range of the $\eta^4\text{He}$ interaction, as given by the empirical density of the ^4He nucleus. The results lead to a bump structure of $|T|^2$ below threshold, closely related to the shape of the $\eta^4\text{He}$ production cross sections close to threshold.

The potential and other parameters related to the production vertices are fitted to the data and in this way we deduce that there is a peak of $|T|^2$ below threshold which roughly can be parametrized in a Breit-Wigner form suggestive of an $\eta^4\text{He}$ bound state. Certainly, this structure is tied to the fast increase of the $dd \rightarrow \eta^4\text{He}$ cross sections close to threshold. However, within the uncertainties of the fit to the data, we found poles in the unbound energy region, in the bound region or no poles at all. Yet, we could quantize the probability to have a pole in the bound region in 62%. We also obtain an $\eta^4\text{He}$ scattering length of the order of $[(2.6 \pm 0.8) - i(1.1 \pm 0.4)]$ fm.

In summary, the new approach to the analysis of the $dd \rightarrow \eta^4\text{He}$ data close to threshold has proved quite useful and has been able to provide information on a bound state of the $\eta^4\text{He}$ system. It remains to be seen if this structure could be seen in some experiments. The broad shape of $|T|^2$ in Figs. 6 and 7 would not make the matter easy, and in addition one should take into account that large contributions of background source from reactions not tied to the possible bound state formation would further blur a signal. Yet, the message we found from the analysis is that due to the limited data and the large errors in the fit, we find that these data cannot confirm nor rule out the existence of poles in the bound region, which would correspond to $\eta^4\text{He}$ bound states. In any case, in case where bound states appear we still see the general rule that the widths are larger than the binding energies. Nevertheless, a peak structure of $|T|^2$ below threshold seems unavoidable and it is linked to the fast raise of the $dd \rightarrow \eta^4\text{He}$ cross sections close to the reaction threshold.

Acknowledgments

We would like to express our thanks to Michael Döring for useful discussions with him. This work is partly supported by the National Natural Science Foundation of China (Grants No. 11475227, No. 11735003, No. 11565007, and No. 11747307) and the Youth Innovation Promotion Association CAS (No.

2016367). This work is also partly supported by the Spanish Ministerio de Economía y Competitividad and European FEDER funds under the contract number FIS2014-57026-

REDT, FIS2014-51948-C2- 1-P, and FIS2014-51948-C2-2-P, and the Generalitat Valenciana in the program Prometeo II-2014/068.

-
- [1] C. Wilkin, *Acta Phys. Polon. B* **47**, 249 (2016).
 - [2] S. D. Bass and P. Moskal, *Acta Phys. Polon. B* **47**, 373 (2016).
 - [3] Q. Haider and L. C. Liu, *Int. J. Mod. Phys. E* **24**, 1530009 (2015).
 - [4] N. G. Kelkar, *Acta Phys. Polon. B* **46**, 113 (2015).
 - [5] S. Hirenzaki, H. Nagahiro, N. Ikeno, and J. Yamagata-Sekihara, *Acta Phys. Polon. B* **46**, 121 (2015).
 - [6] E. Friedman, A. Gal, and J. Mareš, *Phys. Lett. B* **725**, 334 (2013).
 - [7] R. S. Bhalerao and L. C. Liu, *Phys. Rev. Lett.* **54**, 865 (1985).
 - [8] Q. Haider and L. C. Liu, *Phys. Lett. B* **172**, 257 (1986).
 - [9] L. C. Liu and Q. Haider, *Phys. Rev. C* **34**, 1845 (1986).
 - [10] H. C. Chiang, E. Oset, and L. C. Liu, *Phys. Rev. C* **44**, 738 (1991).
 - [11] T. Inoue and E. Oset, *Nucl. Phys. A* **710**, 354 (2002).
 - [12] C. Garcia-Recio, J. Nieves, T. Inoue, and E. Oset, *Phys. Lett. B* **550**, 47 (2002).
 - [13] A. Cieplý, E. Friedman, A. Gal, and J. Mareš, *Nucl. Phys. A* **925**, 126 (2014).
 - [14] N. Barnea, E. Friedman, and A. Gal, *Phys. Lett. B* **747**, 345 (2015).
 - [15] N. Barnea, E. Friedman and A. Gal, *Nucl. Phys. A* **968**, 35 (2017).
 - [16] J. J. Xie, W. H. Liang, E. Oset, P. Moskal, M. Skurzok and C. Wilkin, *Phys. Rev. C* **95**, 015202 (2017).
 - [17] R. Bilger *et al.*, *Phys. Rev. C* **65**, 044608 (2002).
 - [18] T. Mersmann *et al.*, *Phys. Rev. Lett.* **98**, 242301 (2007).
 - [19] C. Wilkin *et al.*, *Phys. Lett. B* **654**, 92 (2007).
 - [20] J. Urban *et al.* [COSY-GEM Collaboration], *Int. J. Mod. Phys. A* **24**, 206 (2009).
 - [21] R. Frascaria *et al.*, *Phys. Rev. C* **50**, R537 (1994).
 - [22] N. Willis *et al.*, *Phys. Lett. B* **406**, 14 (1997).
 - [23] A. Wronska *et al.*, *Eur. Phys. J. A* **26**, 421 (2005).
 - [24] M. Skurzok, P. Moskal and W. Krzemien, *Prog. Part. Nucl. Phys.* **67**, 445 (2012).
 - [25] P. Adlarson *et al.* [WASA-at-COSY Collaboration], *Phys. Rev. C* **87**, 035204 (2013).
 - [26] W. Krzemień *et al.* [WASA-at-COSY Collaboration], *Acta Phys. Polon. B* **45**, 689 (2014).
 - [27] W. Krzemień *et al.* [WASA-COSY Collaboration], *Acta Phys. Polon. B* **46**, 757 (2015).
 - [28] M. Skurzok *et al.* [WASA-at-COSY Collaboration], *Acta Phys. Polon. B* **47**, 503 (2016).
 - [29] P. Adlarson *et al.*, *Nucl. Phys. A* **959**, 102 (2017).
 - [30] R. E. Chrien *et al.*, *Phys. Rev. Lett.* **60**, 2595 (1988).
 - [31] J. D. Johnson *et al.*, *Phys. Rev. C* **47**, 2571 (1993).
 - [32] G. A. Sokol, T. A. Aibergenov, A. V. Kravtsov, A. I. L'vov, and L. N. Pavlyuchenko, *Fizika B* **8**, 85 (1999).
 - [33] A. Budzanowski *et al.* [COSY-GEM Collaboration], *Phys. Rev. C* **79**, 012201 (2009).
 - [34] P. Moskal and J. Smyrski, *Acta Phys. Polon. B* **41**, 2281 (2010).
 - [35] F. Pheron *et al.*, *Phys. Lett. B* **709**, 21 (2012).
 - [36] H. Fujioka *et al.* [Super-FRS Collaboration], *Acta Phys. Polon. B* **46**, 127 (2015).
 - [37] T. Rausmann *et al.*, *Phys. Rev. C* **80**, 017001 (2009).
 - [38] N. Ikeno, H. Nagahiro, D. Jido and S. Hirenzaki, *Eur. Phys. J. A* **53**, 194 (2017).
 - [39] M. Skurzok, P. Moskal, N. G. Kelkar, S. Hirenzaki, H. Nagahiro and N. Ikeno, arXiv:1802.08597 [nucl-ex].
 - [40] I. Sick, *Phys. Rev. C* **90**, 064002 (2014).
 - [41] E. Oset and A. Ramos, *Nucl. Phys. A* **635**, 99 (1998).
 - [42] J. Landay, M. Döring, C. Fernández-Ramírez, B. Hu and R. Molina, *Phys. Rev. C* **95**, 015203 (2017).